Supporting Information

Highly efficient and thermal stable Sb_2Se_3 solar cells based on hexagonal CdS buffer layer by environment friendly interface optimization

Huafei Guo[a], Xuguang Jia[b], Shreyash H. Hadke[d], Jiayi Zhang[a], Wei Wang[e], Changhao Ma[b], Jianhua Qiu[a], Ningyi Yuan[b], Lydia H. Wong*[d] and Jianning Ding*[c]*

Lattice mismatch is unavoidable in heterojunctions, inducing a large number of dangling bonds atthe interface. For an abrupt heterojunction, its dangling bonds at the interface can beestimated by calculating the bond density difference between the two materials at the interface, which is:

$$\Delta N_s = N_{s1} - N_{s2} \quad (1)$$

where N_{s1} and N_{s2} are the bond density of two materials at the interface and are determined by the lattice constant and surface orientation. It can be seen from XRD and TEM that the [221]-oriented Sb_2Se_3 film grows on a (002) plane of H-CdS and (111) plane of C-CdS, respectively. Therefore, we build atomistic models of Sb_2Se_3, H-CdS and C-CdS bulk crystals, cleave these surfaces and optimize their lattice parameters by first-principles calculations. Fig. 1(g) and 1(h) show the schematic of the growth of Sb_2Se_3 film with a (221) orientation deposited on C-CdS and H-CdS film. It can be seen the bond density of C-CdS (111) plane is around twice of the H-CdS (002) plane. The lattice parameters after geometry optimization and bond density are listed in Table 1. According to Equation 1, the dangling bonds density of Sb_2Se_3(221)/H-CdS(002) interface and Sb_2Se_3(221)/C-CdS(111) are $1.6 \times 10^{13} cm^{-2}$ and $6.53 \times 10^{14} cm^{-2}$, respectively. It can be seen that the dangling bond density at the

Sb_2Se_3(221)/C-CdS(111) interface is more than 10 times larger than that at the Sb_2Se_3(221)/H-CdS(002) interface.Therefore, in terms of dangling bonds, the defect density of Sb_2Se_3(221)/C-CdS(111) interface is much larger than that of the Sb_2Se_3(221)/H-CdS(002) interface, which is consistent with our experiment results. It should be noted that this overly simple estimation does not consider the effect of different thermal expansion coefficients of the two materials or the interface states introduced by the mutual diffusion of elements and possible surface reconstruction, and should serve only as a rule of thumb.

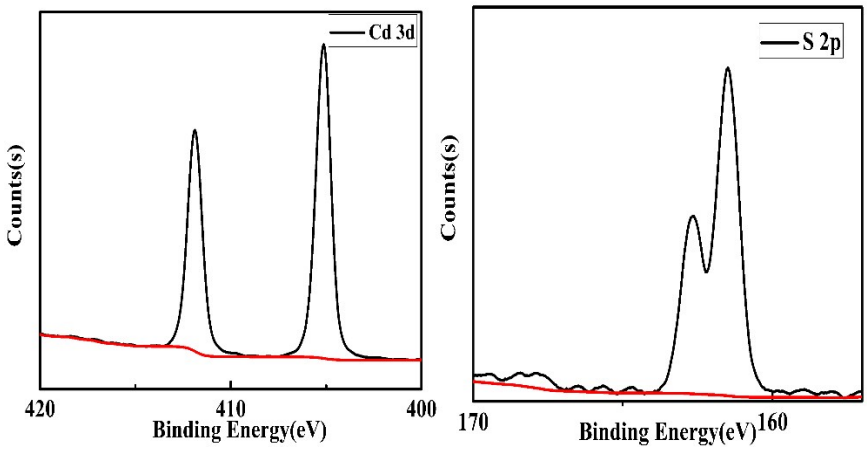

FigS1 The XPS of hexagonal CdS(H-CdS) film

Table S1 the electrical properties of C-CdS and H-CdS film

Sample	Resistivity (Ohm*cm)	Mobility (cm^2/Vs)	Carrier concentration (cm^{-3})	Carrier type
C-CdS	3.27	-4.02	-4.73E+17	N
H-CdS	0.0815	-1.75	-4.36E+19	N

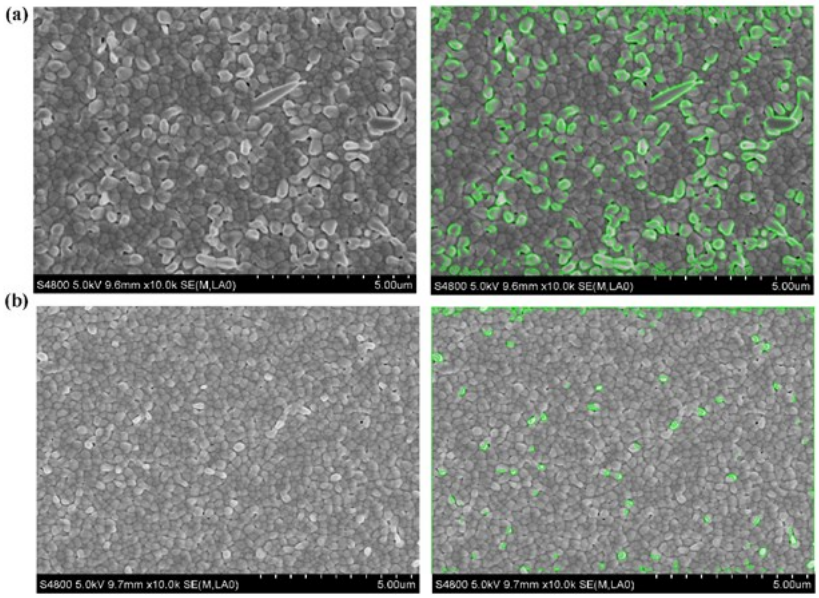

Fig S2 The surface SEM images of Sb_2Se_3 film based on (a) C-CdS film and (b) H-CdS film

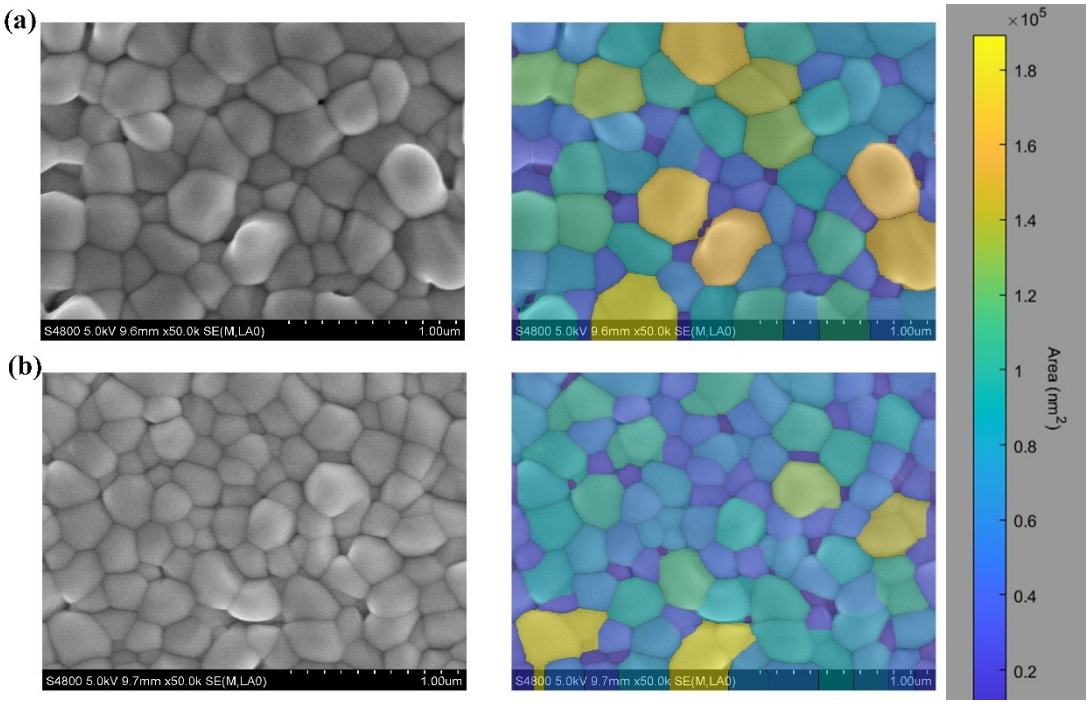

Fig S3 The grain size Sb_2Se_3 films based on (a) C-CdS and (b) H-CdS film

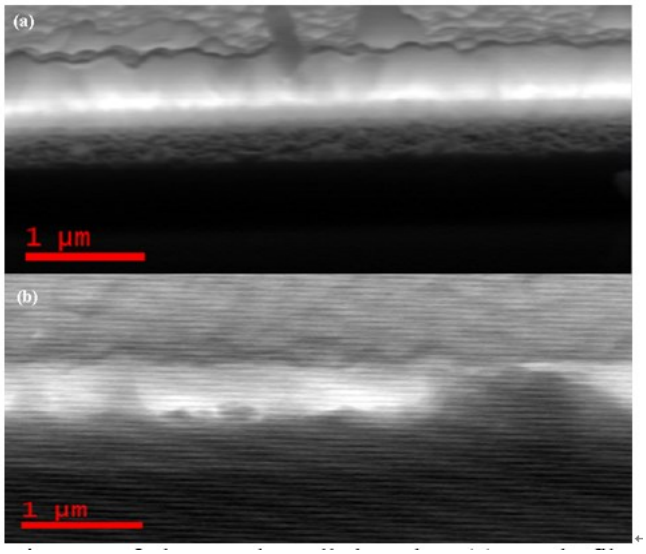

Fig S4 The EBICimages of Sb_2Se_3 solar cells based on (a) C-CdS film,(b) H-CdS film

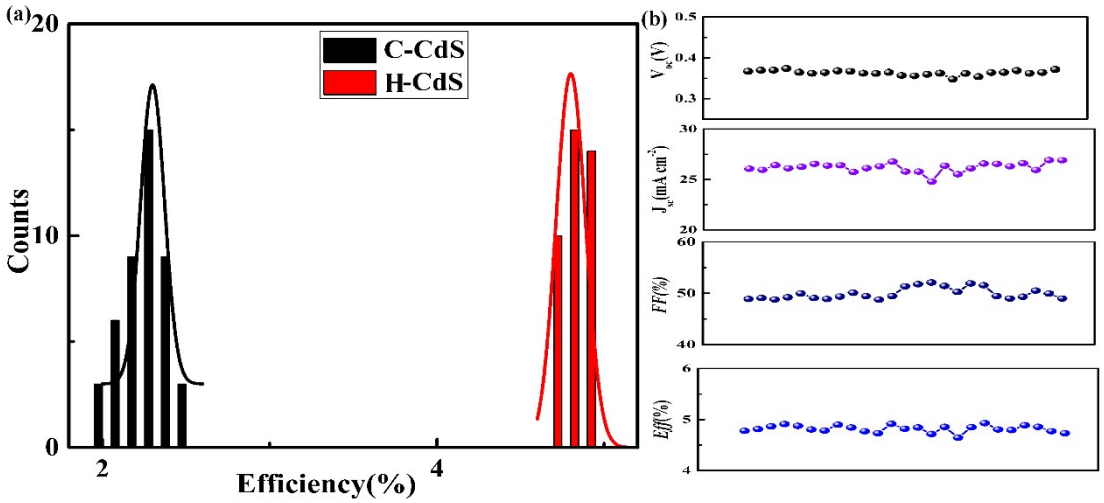

Fig S5 A histogram of the *J–V* scan efficiencies of Sb_2Se_3 solar cells based on C-CdS and H-CdS film

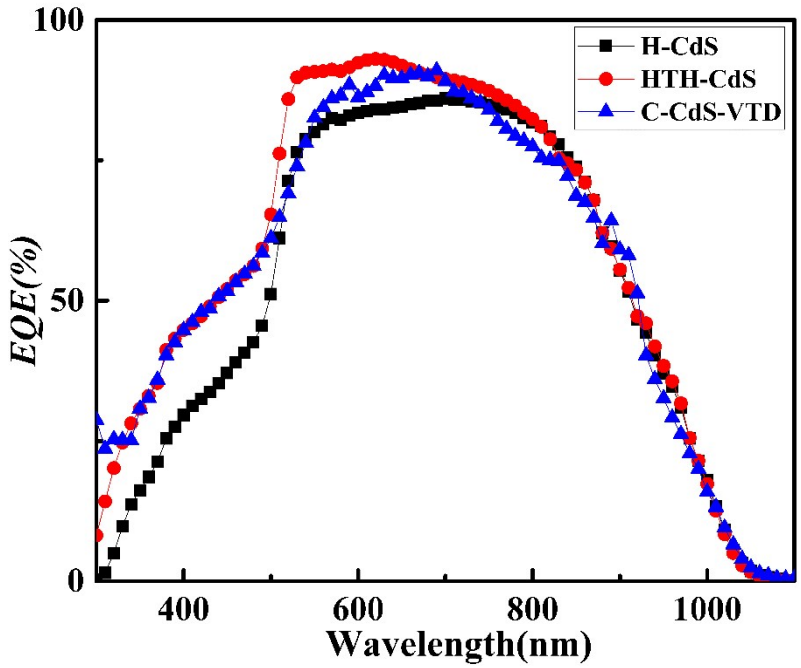

Fig S6 The *EQE* of Sb_2Se_3 solar cells based on RTE and VTD method, the RTE is based on H-CdS film, the VTD is based on C-CdS film

Fig S7 The picture of H-CdS film (a) as-deposited, (b) 500°C annealing and (c) 600°C annealing

Tbale.S2 The element composition of CdS films with and without 500^{o}C heating treatment

Sample	Cd (at%)	S (at%)	O (at%)
H-CdS	35.50	40.82	23.67
HTH-CdS	28.87	30.89	40.24

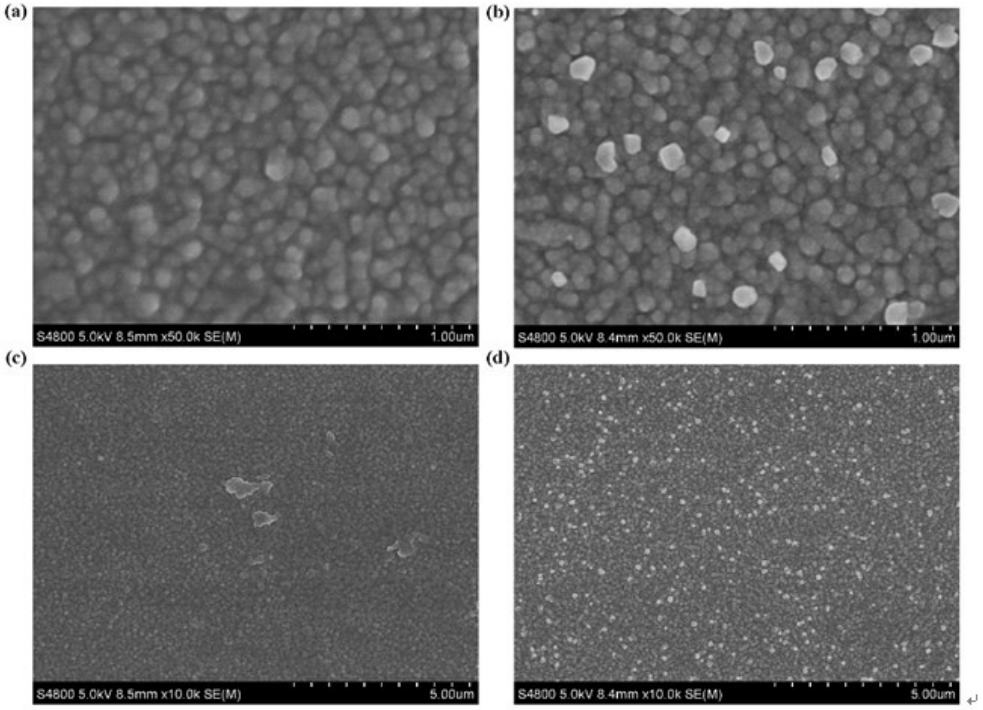

Fig S8 The surface SEM images of (a), (c) H-CdS and (b), (d) HTH-CdS film

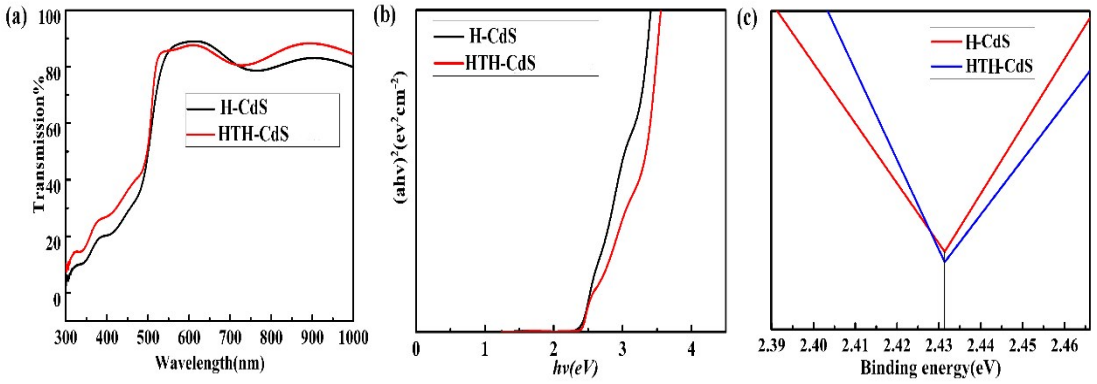

Fig S9 (a) The Transmission and (b) band gap of CdS film with and without annealing treatment, (c) the band gap of H-CdS and HTH-CdS film derivative from the *EQE* result

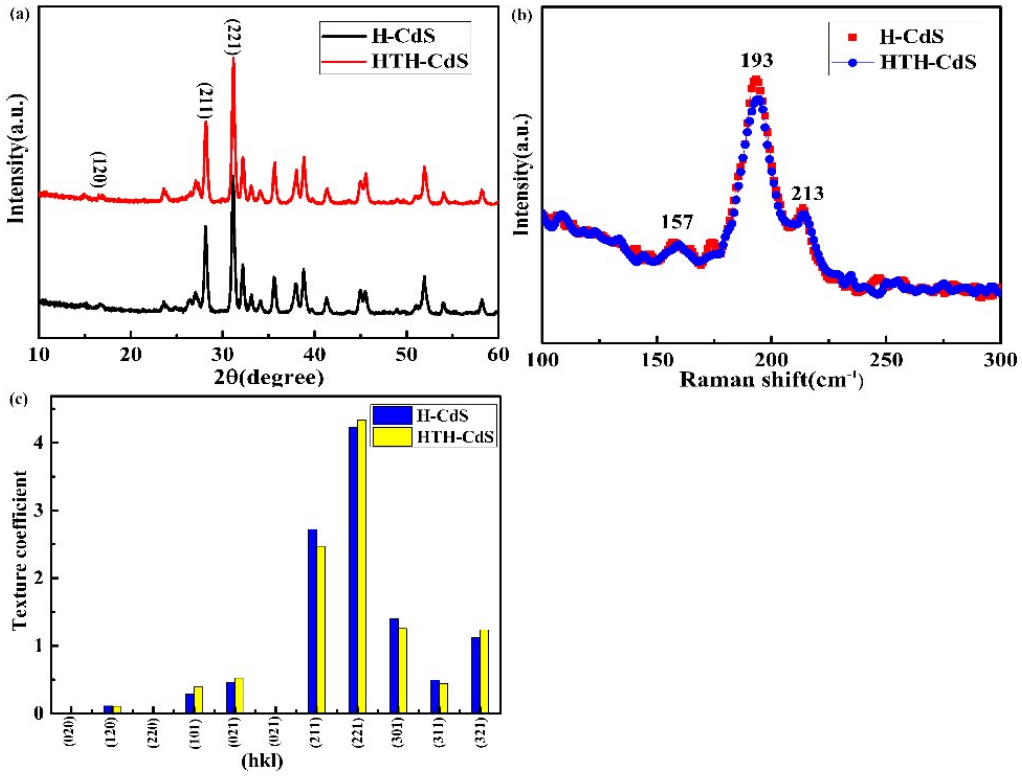

Fig S10 The (a) XRD, (b) Raman and (c) Texture coefficient patterns of Sb_2Se_3 solar cells based on H-CdS and HTH-CdSfilm

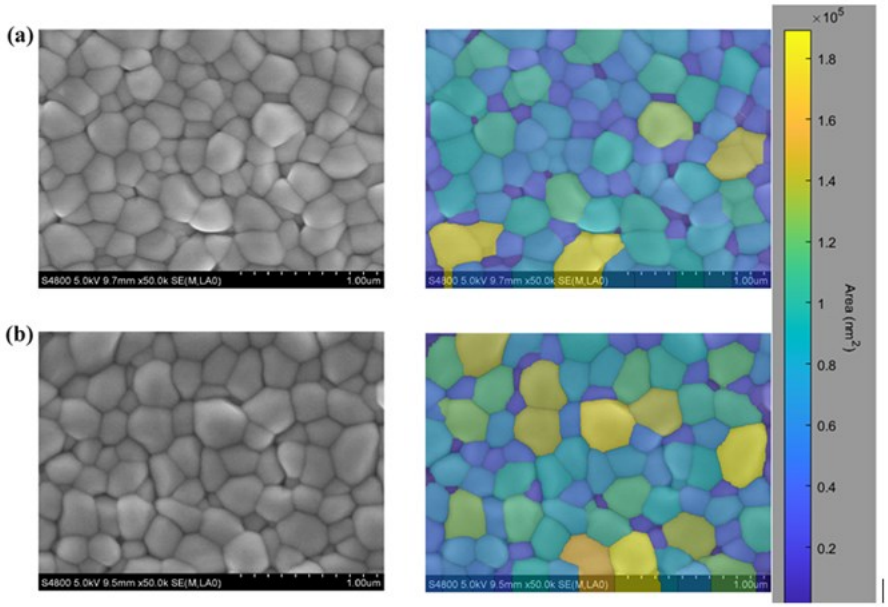

Fig S11 The surface SEM images and grain sizes of Sb_2Se_3 film based on (a) H-CdS and (b) HTH-CdS film

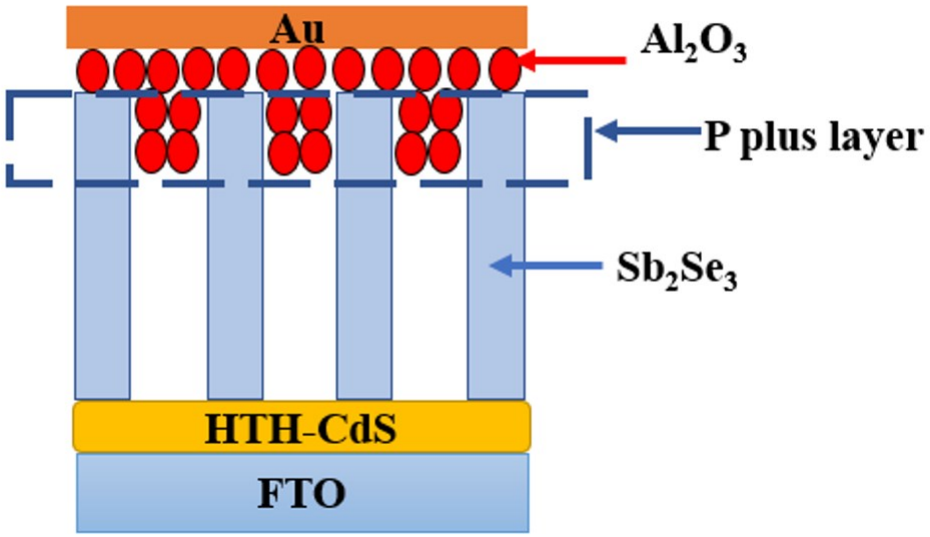

Fig S12 The diagrammatic structure of the device with adding of Al_2O_3 layer

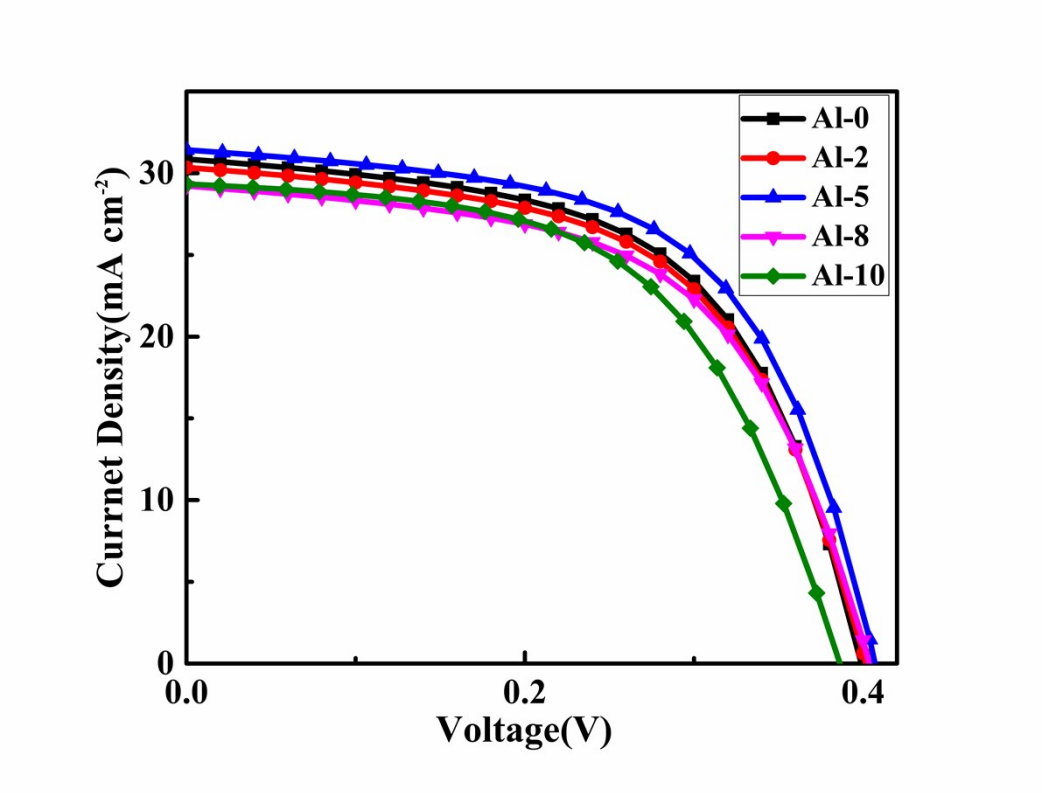

Fig S13 The efficiency of Sb_2Se_3 solar cells based on different pre-heating time

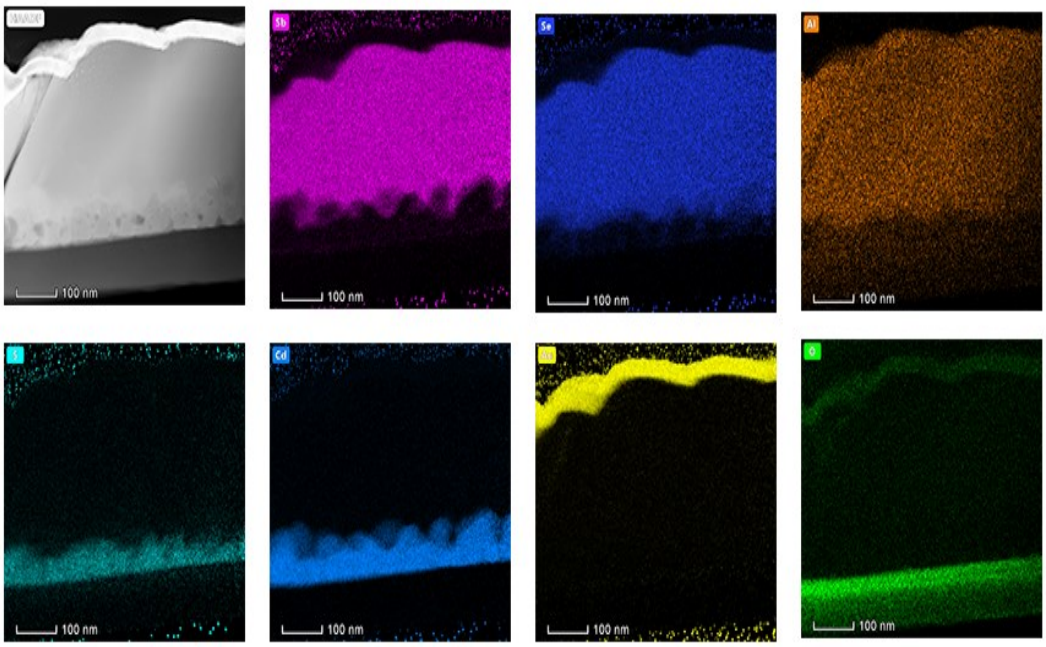

Fig S14 The cross-sectional TEM mapping of Sb_2Se_3 solar cells based on 5min pre-heating treatment

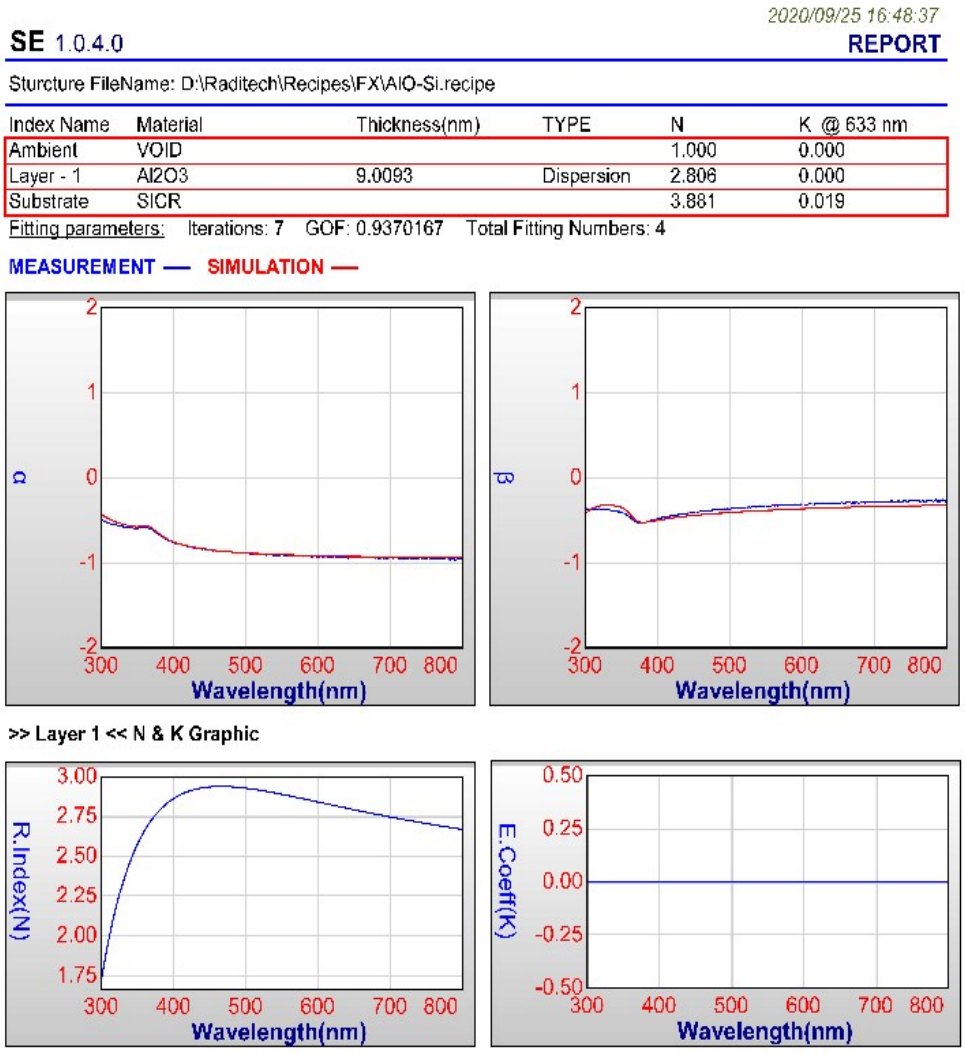

Fig S15 The ellipsometry result of Al_2O_3 layer with 90 cycle

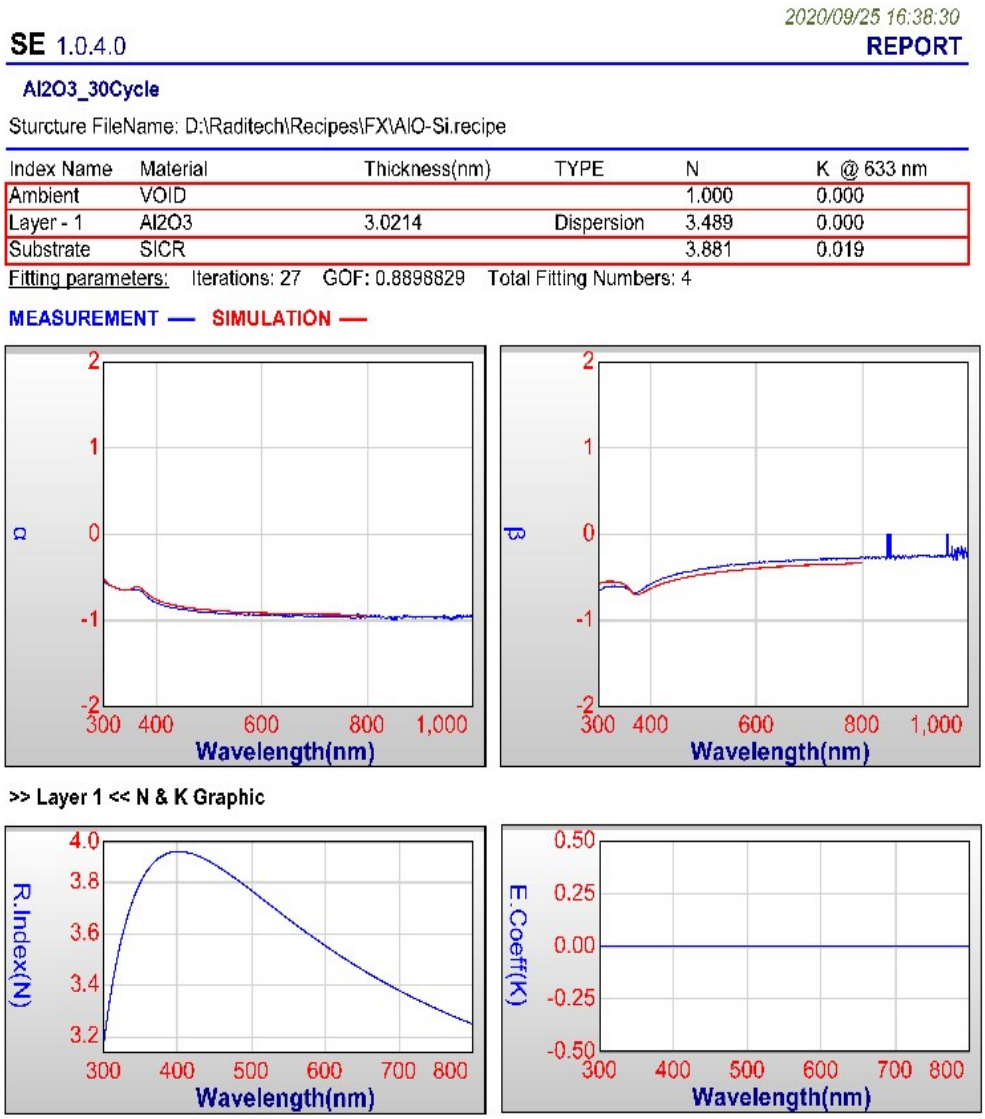

Fig S16 The ellipsometry result of Al_2O_3 layer with 30 cycle

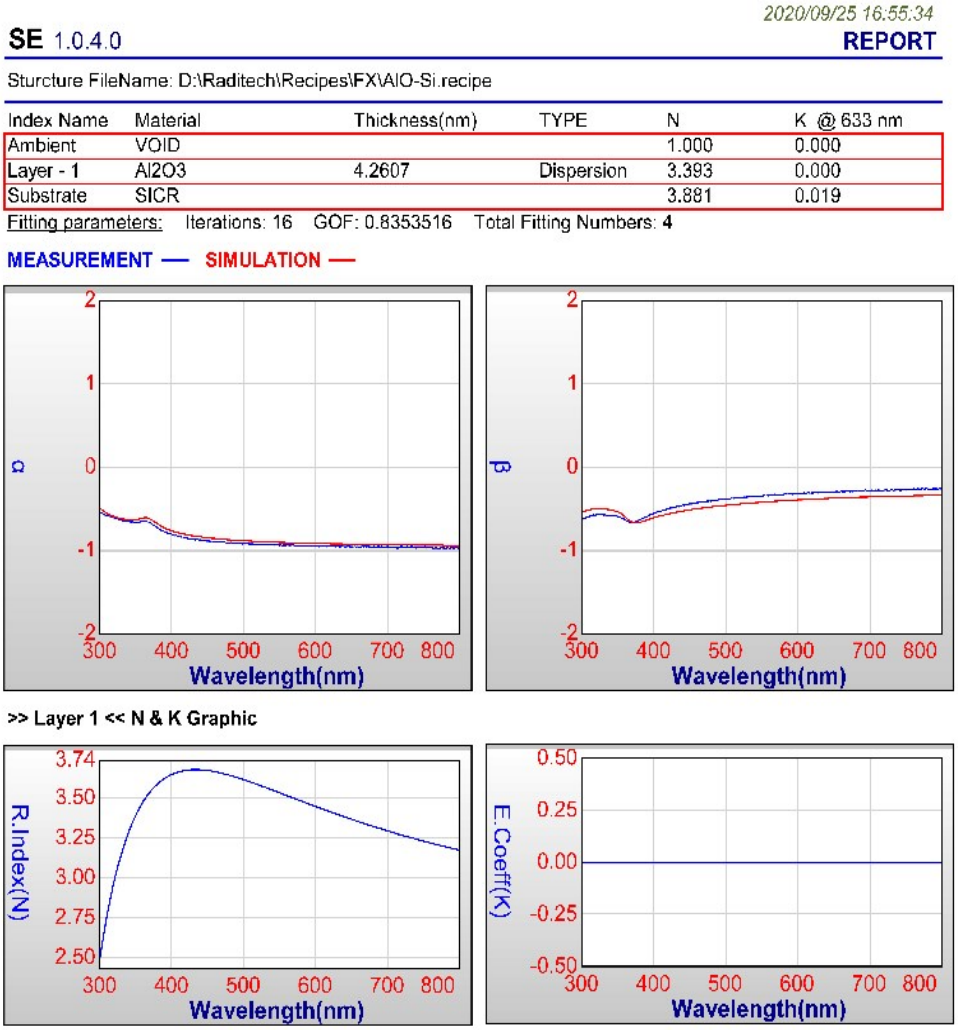

Fig S17 The ellipsometry result of Al_2O_3 layer with 42 cycle

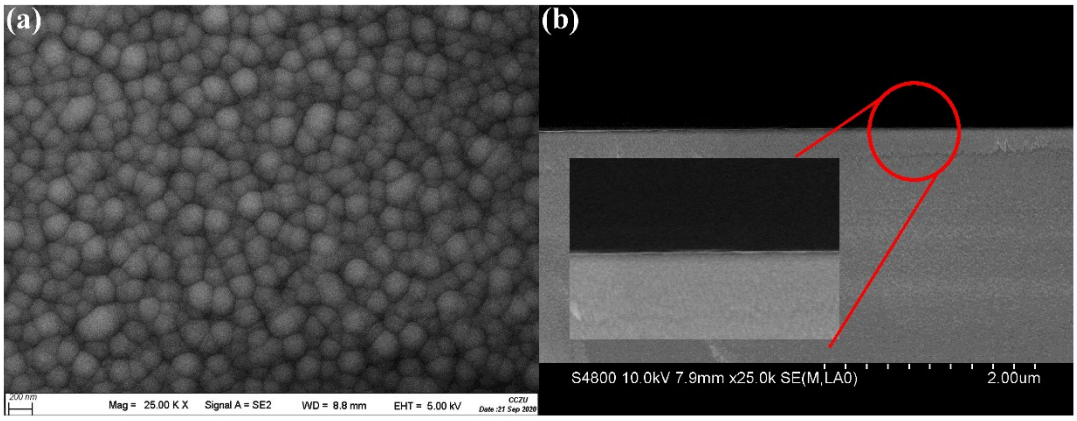

Fig S18 The surface and cross-sectional SEM images of pure Al_2O_3 layer

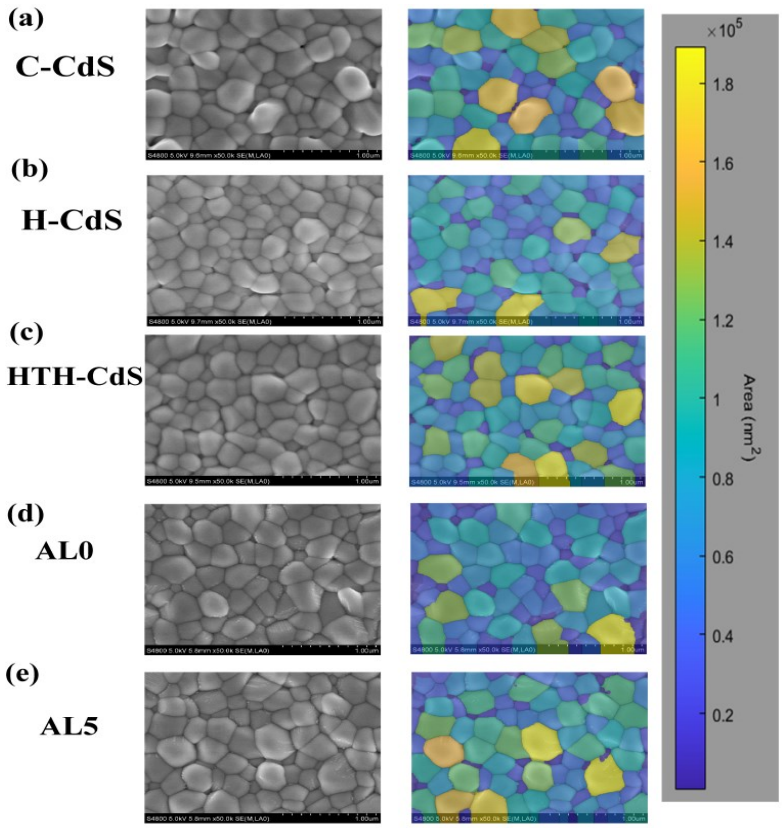

Fig. S19 The surface SEM images and grain sizes of Sb_2Se_3 films based on (a) C-CdS, (b) H-CdS, (c) HTH-CdS, (d) AL-0 and (e) AL-5

Fig S19 shows the grain sizes of Sb_2Se_3 film under different conditions, and it can be seen clearly the grain size of Sb_2Se_3 increased with the moving forward of our experiment which implying a low grain boundary density of the device. This results also indicates that the H-CdS film can totally replace C-CdS film to fabricating high efficiency Sb_2Se_3 thin film solar cells.